Residual Stresses in Flash Butt Welded Rail†

CAI Zhipeng*, NAWAFUNE Masashi, MA Ninshu ***, QU Yuebo****, CAO Bin**** and MURAKAWA Hidekazu*****

Abstract

The residual stresses on the surface of a rail joined by flash-butt welding are measured using a hole-drilling method and the thermal elastic-plastic deformation process considering the phase transformation are simulated using FEM code JWRIAN. The residual stresses measured by experiments and computed by FEM have an acceptable agreement in accuracy. The simulation results show that the phase transformation in the cooling stage has a significant effect on the residual stress distribution and its values. The tensile or compressive state for residual stresses near the welding section strongly depends on the phase transformation which occurred during the cooling process. The biaxial tensile stresses are produced at the web near the fusion line of the flash butt welded rail. The biaxial tensile stresses increase the risk of cracks. Although the Martensite phase transformation during the cooling process at top and bottom near the fusion line produces compressive stress, it increases the brittleness at the same time. Therefore, the proper heat treatment after welding is still necessary in order to improve the toughness.

KEY WORDS: (Flash butt welding), (U71Mn Rail), (Residual Stress), (Phase Transformation), (Measurement), (FEM Simulation)

1. Introduction

Compared with traditional bolt joining for rail, the welded rail has a continuity of joint geometry which can reduce the impact load and structural vibration of high speed trains.

Generally, the flash butt welding is mainly used for the joining of the rails. However, the un-uniformly distributing mechanical properties and residual stresses in the welded zone and heat affected zone of a welded rail joint may have a bad influence on the cracks and fatigue life under service loading conditions[1]. **Figure 1** shows an example where a crack occurred in the web of a welded rail joint.

To investigate the reasons for cracks due to butt flash welding in the web, residual stresses are predicted by numerical simulation and verified by experimental measurements. Furthermore, phase transformation is considered in the simulation model for the prediction of Martensite phase fraction in the welded zone and for the improvement of prediction accuracy for residual stresses.

Relating to the measurement of residual stresses in the rail joints of flash butt welding, some research achievements have been obtained[2-7]. H. Mansouri et al[2] measured the residual stresses in a welded rail made by a standard gap alumino-thermic process using a Neutron strain scanning method. David Tawfika et al[3] used the neutron diffraction method and investigated residual stresses in an AS60 flash butt welded rail. Kingston et al[4] measured the through-thickness residual stress distributions of the flush butt welded rail using deep-hole drilling method. A.Skyttebol[5] measured residual stresses on the surface of the welded rail using the hole-drilling strain method.

All these measured results show that the original stresses before welding are tensile in the head and foot of

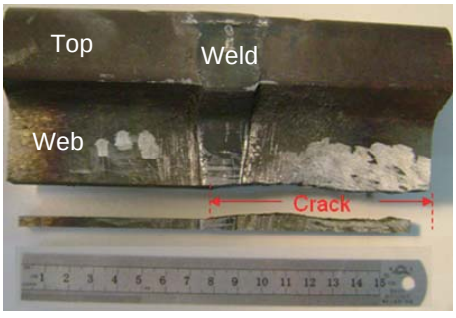

Fig. 1 Crack in the web of a rail joint.

† Received on June 10, 2011
* Associate Professor, Tsinghua University
** Graduate Student
*** Guest Associate Professor
**** Graduate Student, Tsinghua University
*****Professor

Transactions of JWRI is published by Joining and Welding Research Institute, Osaka University, Ibaraki, Osaka 567-0047, Japan

rail and compressive in the web. After welding, the residual stress distributions are very complex. On the top and bottom surfaces of the rail, the longitudinal residual stress produced by welding is compressive, which is generally good for preventing the initiation and propagation of fatigue cracks. In the web region, both longitudinal and vertical components of the residual stress are tensile, which may increase the possibility of crack initiation and propagation.

To explain the difference of the residual stresses on the head, foot and web of the welded rail, H. Mansouri and A. Monshi[6] observed the microstructure and measured surface residual stresses near the welded zone. It was observed that the temperature at the web is higher than the temperature at the head and foot of the rail just after flash butt welding finished. During cooling, the contraction at the web with higher temperature is constrained by both the head and foot of the rail. Therefore, the tensile residual stresses are produced in the web after cooling. In the head and foot of the rail, compressive residual stresses are developed.

A few of simulation works for the welding stresses in rails are also performed[1, 5, 7]. David Tawfika et al[1] used an approximate thermal model and analyzed the residual stresses in the AS60 and AS68 welded rail using a thermo-mechanical finite element method (FEM). A. Skyttebol et al[5, 7] proposed a FEM model in which the welding temperature field was firstly computed using the electric thermal analysis and then the thermo-mechanical analysis for stress and strain fields was conducted.

However, all these studies did not discuss the effect of phase transformation on the residual stress distribution and the plastic strain history near the fusion zone, which is very important for the residual stress value and its distribution. In this research, the residual stresses at some focused positions of the rail are measured by hole-drilling method, and the residual stresses and Martensite phase fraction in the welded joint are predicted by FEM code JWRIAN. The results show that the phase transformation in the cooling process has a significant influence on the residual stress value and plastic strain history. Biaxial tensile residual stresses and the brittle Martensite microstructure existing in the web of the welded rail are predicted. These may be the main reasons for the cracking in the web. The biaxial tensile residual stresses in the web predicted by FEM simulation considering phase transformation are coincident with the measured ones.

2. Experiments of Rail Flash Butt Welding

2.1 Material and shape of U71Mn rail

The material of the rail is U71Mn. Its chemical composition is listed in **Table 1** and the section shape of the rail is show in **Fig. 2**, respectively[9].

2.2 Flash butt welding conditions

Two U71Mn rails with 1000 mm in length were welded by flash butt welding process using the same welding conditions shown in **Fig. 3**. The Upper curve, middle curve and lower curve show the changes in the squeezing force, welding current and relative displacement between the two ends of the welded rail with time during welding, respectively.

3. Modeling of FEM Simulation

3.1 Mesh division

The mesh for the rail flash-butt welded joint used in simulation is shown in **Fig. 4**. There are 34,320 elements and 39,556 nodes. The minimum mesh size is about 2 mm in length near welded center line.

Table 1 Chemical composition of U71Mn rail (wt%).

C		Si	Mn	S	P	Fe
0.67 0.74	~	0.26~0.3	1.3~1.4	0.02~0.04	0.02~0.04	The rest

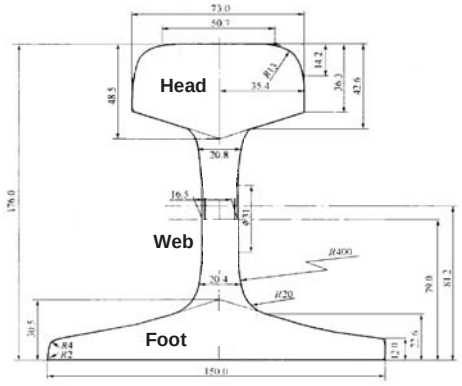

Fig. 2 Section shape of the U71Mn rail.

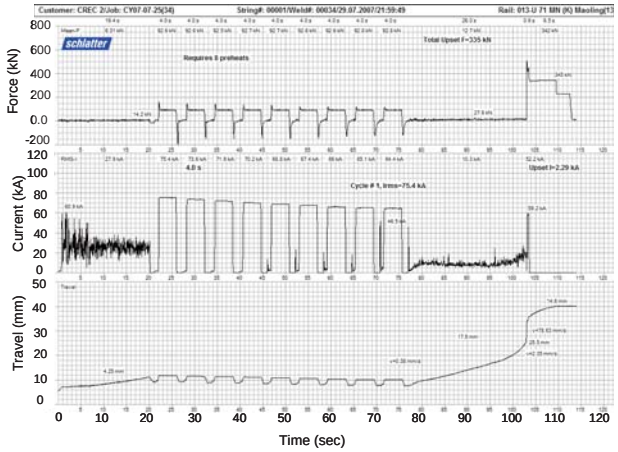

Fig. 3 Typical parameters of flash-butt welding for rail.

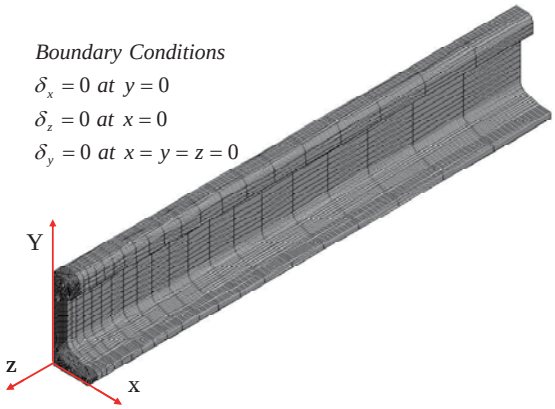

Fig. 4 Mesh and boundary conditions for FEM.

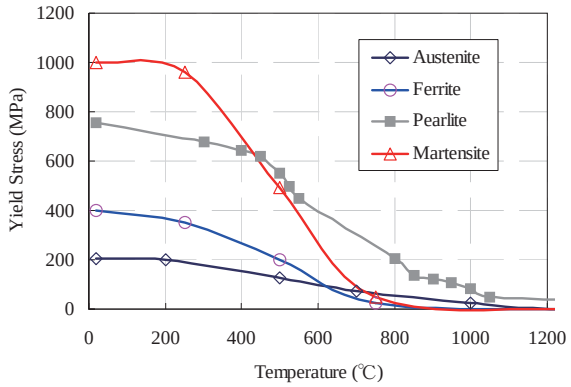

Fig. 5 Yield strength with temperature for various micro-structures.

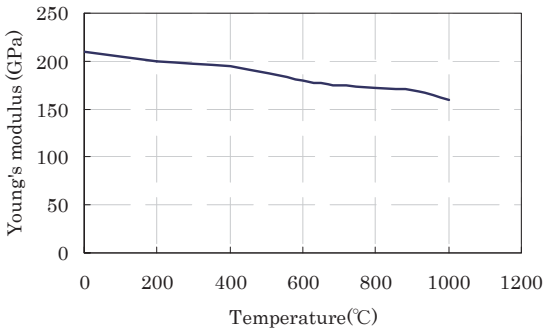

Fig. 6 Elastic modulus with temperature.

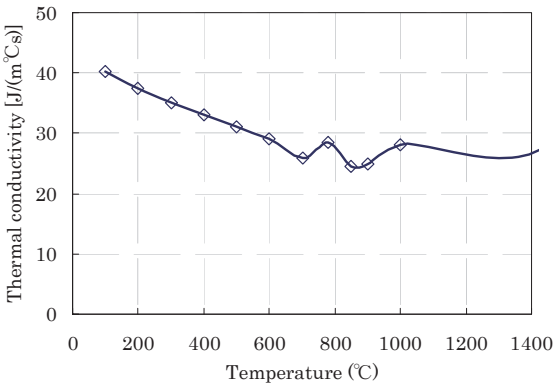

Fig. 7 Thermal conductivity with temperature.

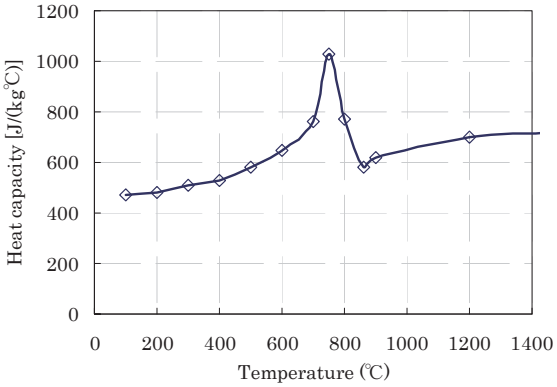

Fig. 8 Heat capacity with temperature.

3.2 Materials properties

The curves of temperature dependent yield strength for the four kinds of microstructure (Austenite, Ferrite, Pearlite and Martensite) are shown in **Fig. 5**. The original micro-structure of 71Mn rail material is Pearlite. If the phase transformation is not considered in the simulation, only the curve for Pearlite is used.

Figure 6 shows the temperature dependent Young's modulus. **Figures 7**, **8**, **9** and **10** show the changes of thermal conductivity λ, heat capacity C, equivalent heat transfer coefficient β including both convection and radiation of surfaces heat transfer, and thermal expansion coefficient α, respectively.

The density and poisson's ratio are assumed to be $7.80x10^{-06}$ [kg/mm^3] and 0.3, respectively

3.3 Heat source model

Since the continuous-cooling-transformation curve (CCT curve) of U71Mn was not measured, the CCT curve of U75MnV as shown in **Fig. 11**[9] is used to simulate the phase transformation during cooling the simulation. The CCT curve of U71Mn is similar to the CCT curve of U75MnV according to the chemical components.

With consideration of phase transformation, the strain differs with different cooling rate because of expansion caused by generation of Martensite determined by cooling rate. **Figure 12** shows strain history with cooling rate of 1℃/sec, 3 ℃/sec and 10℃/sec, which represent the typical cooling rates for flash butt welding. From **Fig. 11**, it can be known that residual micro-structures are Pearlite only, both Pearlite and Martensite, Martensite only if the cooling rate is 1℃/sec, 3℃/sec and 10℃/sec, respectively. If phase transformation is neglected in the modeling, the strains history for heating and cooling should be the same.

3.4 Heating source model

A volume heat source is adopted in the simulation model. The power and heating time of the volume heat source is determined by the melted region. As shown in **Fig. 3**, the relative displacement between the two ends of rail after welding is 14.6 mm. This means that the melted metal within 14.6 mm was squeezed out. Since a symmetric model is used in the FEM simulation, the metal within 7 mm in longitudinal direction (z), about the half of the whole displacement, was molten during

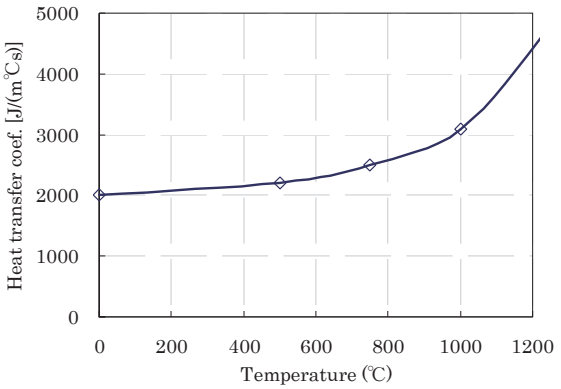

Fig. 9 Heat transfer coefficient including heat convection and radiation changing with temperature.

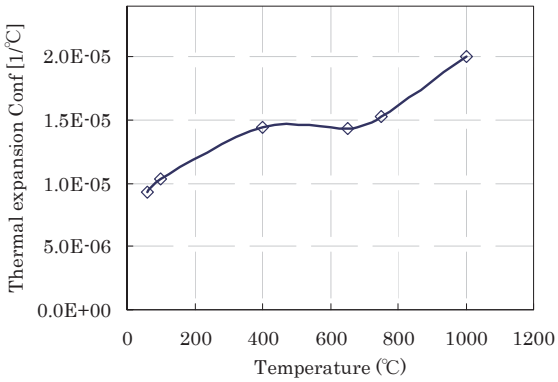

Fig. 10 Thermal expansion coefficient with temperature.

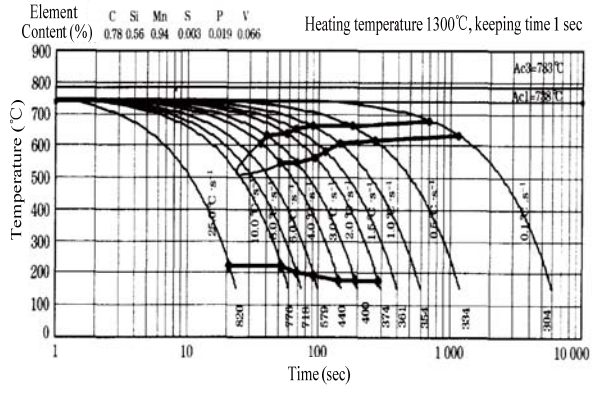

Fig. 11 CCT diagram of U75MnV as the reference.

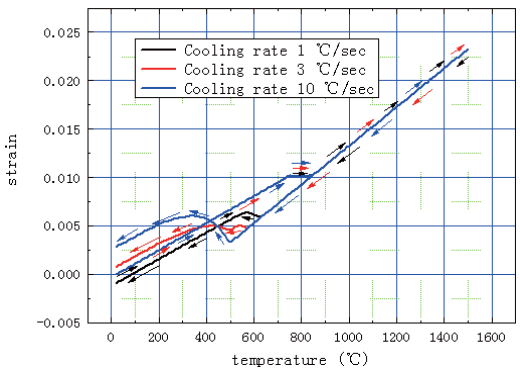

Fig. 12 Stain history with different cooling rate considering phase transformation.

welding and the maximum temperature should be equal to or higher than the melting point 1500℃. Thus, the volume heating model is optimized by viewing maximum reached temperature to make sure that region beyond 1500℃ is near 7 mm in longitudinal direction (z). The elements near the welding center line are heated with input power of 105 [J/s] and heating time of 5 seconds. Such a heat source model could produce a similar temperature fitted with actual results.

3.5 Simulation procedure

The JWRIAN VER. 2010 code is used for the simulation. The simulation procedure is shown in **Fig. 13**[10]. The temperature and phase transformation variation caused by stress are neglected. The temperature changes caused by phase transformation are considered.

4. Residual Stress Measurement

4.1 Measuring method and positions

The residual stresses in three welded joints were measured by a hole-drilling method. The stress measuring areas near the fusion line are shown in **Fig. 14**.

The measuring positions, i.e., the strain gauge attachment positions on the top, web and bottom are shown by **Figs. 15**, **16** and **17**, respectively. Totally, 18 points on the top surface, 18 points on the bottom and 3 points in the wed are measured.

4.2 Measured results

The measured residual stresses on the top and bottom surfaces are listed in **Table 2**. The measured residual stresses on the web surface are listed in **Table 3**. It can be seen that on the top and bottom, the longitudinal residual stress σ_z is compressive. The transverse stress σ_x is small and can be neglected. On the web surface, both the height direction stress σ_y and longitudinal stress σ_z are in the tensile state and the longitudinal stress σ_z is higher. The biaxial tensile stresses on the web surface may increase the possibility of cracks.

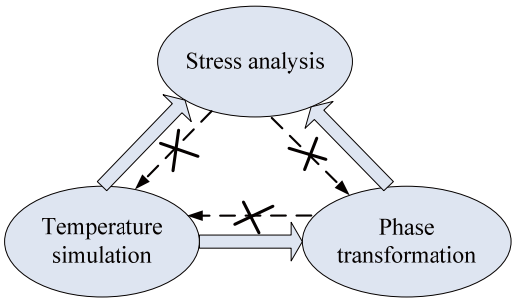

Fig. 13 The relationship among temperature, phase transformation and stress in the simulation.

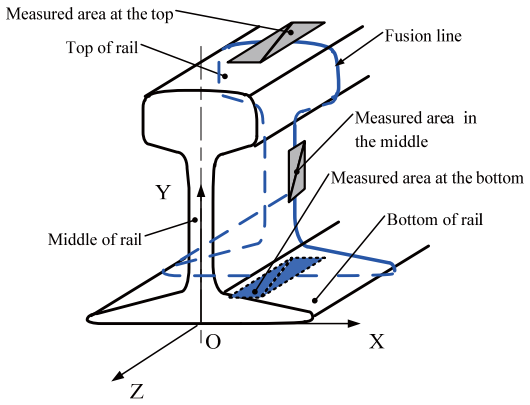

Fig. 14 Stress measuring areas.

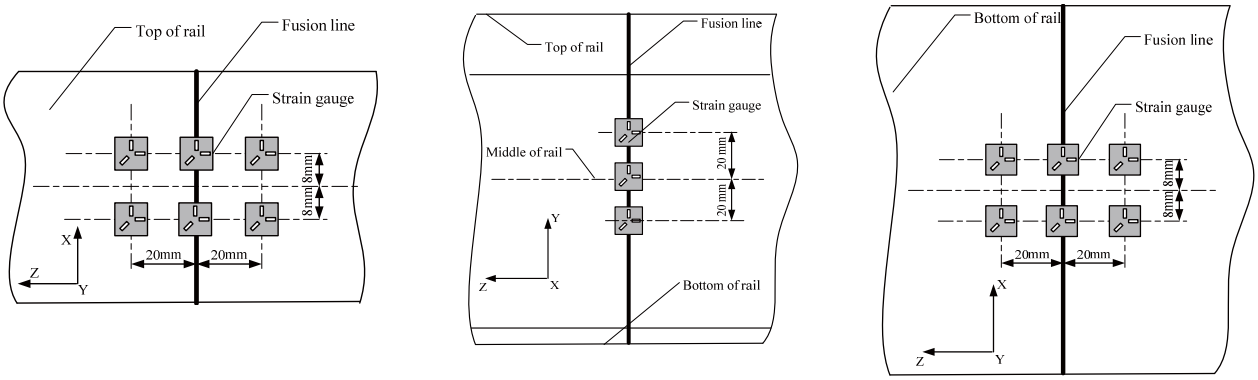

Fig. 15 Strain gauges on top surface of rail. **Fig. 16** Strain gauges on web surface. **Fig. 17** Strain gauges on bottom surface.

Table 2 Residual stresses on the top and bottom surfaces of rail.

Serial number	Distance to fusion line (mm)	Residual stress on top of rail		Serial number	Distance to fusion line (mm)	Residual stress on bottom of rail	
		σ_z/MPa	σ_x/MPa			σ_z/MPa	σ_x/MPa
1-1	-20.00	-253.60	-29.40	1-7	-20.00	-103.30	4.20
1-3	20.00	-283.90	-33.60	1-9	20.00	-159.80	-18.00
1-4	-20.00	-243.50	-11.70	1-10	-20.00	-119.90	-16.50
1-6	20.00	-258.80	-54.30	1-12	20.00	-188.60	-47.50
2-1	-20.00	-179.10	12.20	2-7	-20.00	-132.00	-0.40
2-3	20.00	-267.50	-29.30	2-9	20.00	-115.10	-2.00
2-4	-20.00	-164.70	69.90	2-10	-20.00	-89.80	-1.00
2-6	20.00	-282.30	-21.10	2-12	20.00	-166.60	-33.30
3-1	-20.00	-151.50	48.50	3-7	-20.00	-229.30	-81.40
3-3	20.00	-211.00	-76.20	3-9	20.00	-76.10	25.30
3-4	-20.00	-176.00	29.60	3-10	-20.00	-210.00	-96.50
3-6	20.00	-213.90	-40.20	3-12	20.00	-59.00	53.80
average		-223.82	-11.30	average		-137.46	-17.78
standard error estimate		47.40	43.21	standard error estimate		53.82	42.28

Serial number	Distance to fusion line (mm)	Residual stress on top of rail		Serial number	Distance to fusion line (mm)	Residual stress on bottom of rail	
		σ_z/MPa	σ_x/MPa			σ_z/MPa	σ_x/MPa
1-2	0.00	-214.20	19.50	1-8	0.00	-17.60	57.90
1-5	0.00	-178.00	33.00	1-11	0.00	-84.80	-15.70
2-2	0.00	-189.80	-1.90	2-8	0.00	-45.20	87.10
2-5	0.00	-187.70	68.20	2-11	0.00	-8.50	62.70
3-2	0.00	-306.30	-25.10	3-8	0.00	-65.80	46.80
3-5	0.00	Broken point		3-11	0.00	-110.20	-11.10
average		-215.20	18.74	average		-55.35	37.95
standard error estimate		52.64	35.35	standard error estimate		39.26	41.93

Table 3 Residual stress in the web surface of rail.

Serial number	Distance to middle line of rail (mm)	σ_z (MPa)	σ_y(MPa)
3-13	20	231.5	27.1
3-14	0	217.65	106.25
3-15	-20	167.25	59.95
average		205.47	64.43
standard error estimate		33.81	39.77

5. Simulation Results

5.1 Temperature results

The thermal cycles at three points along the fusion line and at two points in the base metal, 24 mm away from the center line, are shown in **Fig. 18**. The cooling rate at the points on the fusion line is larger than 10℃ /sec.

5.2 Martensite and Pearlite fractions

Figure 19 shows the predicted Martensite fraction after welding. The Martensite fraction is almost 100% within the zone 10 mm away from center line. In the zone 10-12 mm from the center line, the Martensite is about 30% and Pearlite is about 70%. Beyond the zone 12 mm from the center line, the Martensirte is 0% and Pearlite is 100%.

5.3 Residual stress computed by FEM

The computed residual stresses on the fusion line and the section 7 mm away from the fusion line are shown in **Figs. 20** and **21**, respectively. In the figures, “with p.t.” or “without p.t.” means that phase transformation was or

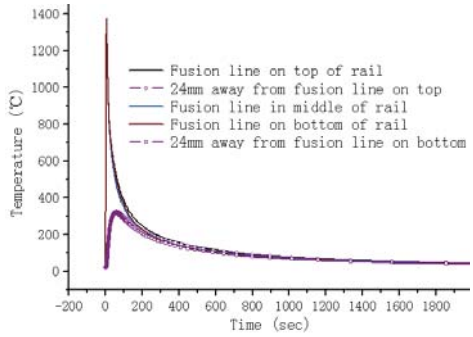

Fig. 18 Thermal cycles at different points.

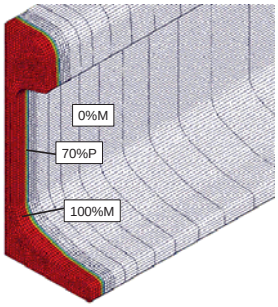

Fig. 19 Martensite and Pearlite fraction after cooling.

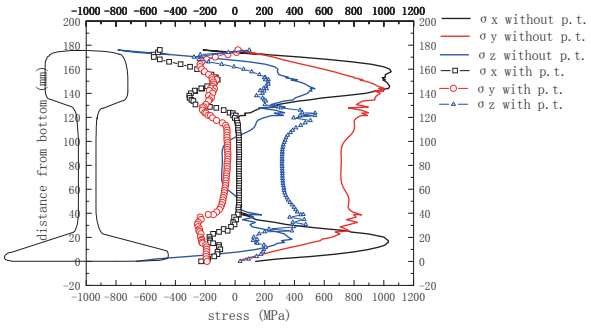

Fig. 20 Computed residual stresses on fusion line and their distributions along height direction.

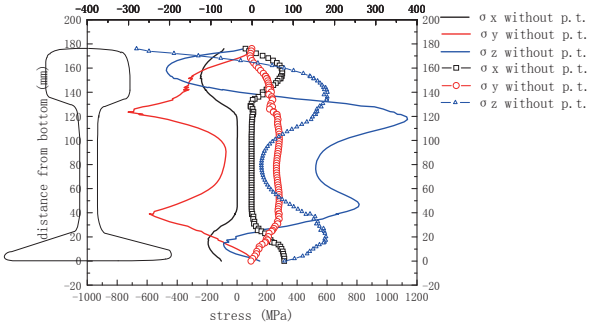

Fig. 21 Computed residual stresses on section 7mm away from fusion line and distributions along height.

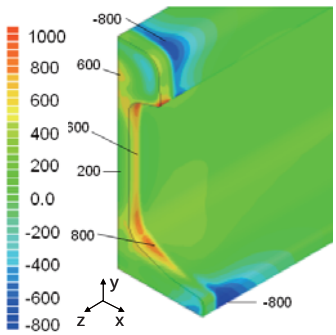

Fig. 22 Residual stress with phase transformation

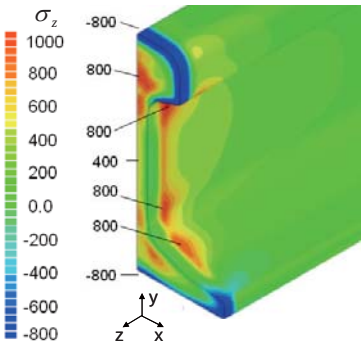

Fig. 23 Residual stress without transformation.

was not considered in the simulation, respectively.

Figures 22 and **23** show the contour distributions of residual stress computed with considering the phase transformation or without considering the phase transformation, respectively. **Figures 24**, **25** and **26** show the distribution of computed residual stress along the longitudinal direction (z) on the top surface, web surface and bottom surface, respectively. In the figures, the measured residual stresses at two points are also represented.

Figure 27 shows the distribution of residual stress along longitudinal direction. It can be seen that the residual stresses computed with and without phase transformation are quite different. Without consideration of the phase transformation the residual stress is much larger than the results with consideration of the phase transformation.

The residual stresses on the location 20 mm away

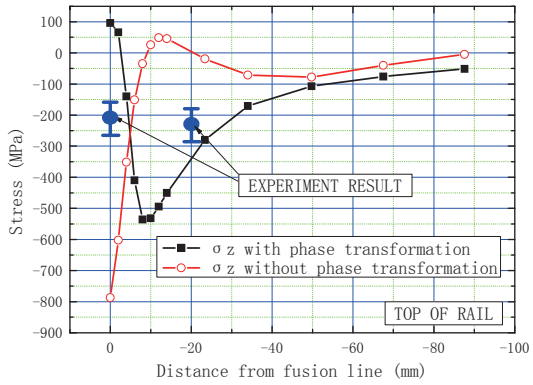

Fig. 24 Comparison of residual stress σ_z on the top of rail between simulation and measurement.

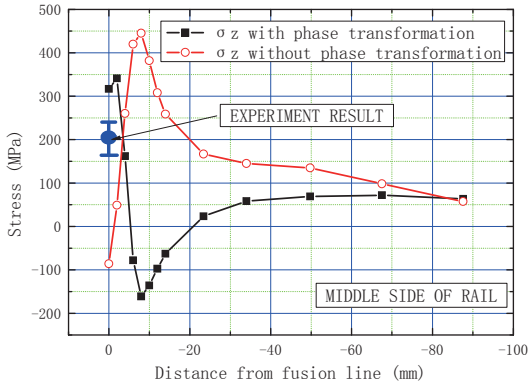

Fig. 25 Comparison of residual stress σ_z on the web of rail between simulation and measurement.

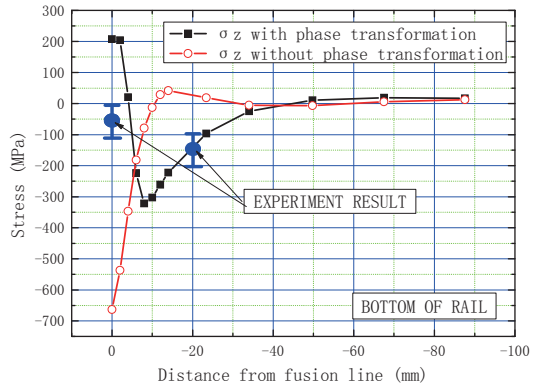

Fig. 26 Comparison of residual stress σ_z on the bottom of rail between simulation and measurement.

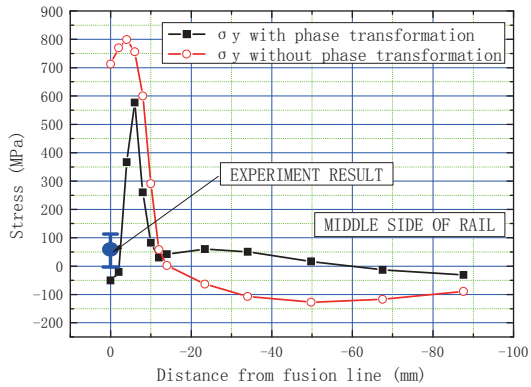

Fig. 27 Comparison of residual stress σ_y on the web of rail between simulation and measurement.

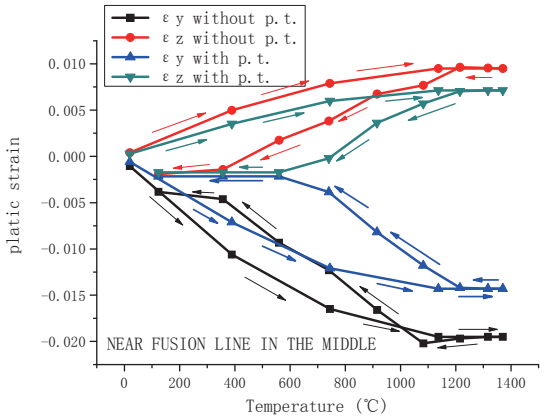

Fig. 28 Plastic strain history in the web during welding with and without phase transformation.

from the fusion line computed with the consideration of the phase transformation show good agreement with measured values. The residual stresses on the fusion line show some difference between computation and measurement.

Both the measured and computed residual stresses on the web near the fusion line are in bi-axial tensile sate. This is an important mechanical reason why the fracture often occurs from the web of rail[9]. The largest tensile residual stress component in the web is σ_y in height direction. This is in coincidence with the normal direction of crack surface observed in experiment as shown in **Fig. 1**.

As shown in **Fig. 28**, both the residual plastic strain ε_y^p and plastic strain ε_z^p are compressive. If the phase transformation is considered in the simulation model, the shape of plastic strain history during the heating path and cooling path become fatter and the residual plastic strains becomes smaller. This is because that the thermal expansion and plastic strain induced by phase transformation occurred during heating and cooling.

From the computed results, it can be concluded that the phase transformation plays an important role for the residual stress distribution caused by flash butt welding. However, there is still a lot of work to improve the modeling precision. For example, the heating process of flash-butt welding could be simulated more realistically. The squeeze force should be considered during heating and cooling.

6. Conclusions

It can be understood from the computed results that the phase transformation plays an important role for the residual stress distribution caused by flash butt welding. By comparing the computed results and experimental results, some conclusions could be drawn as follows,

(1) The computed residual stresses with and without the consideration of the phase transformation are quite different. The model with the phase transformation gave a good result compared with measurement. Therefore, the phase transformation could not be neglected in the simulation of residual stresses produced by flash butt welding.
(2) The bi-axial tensile stress state in the web of welded rail joint increases risk of cracks.
(3) The generation of Martensite during welding and cooling decreases residual tensile stress of joints. However, Martensite increases the metallurgical brittleness of joints at the same time. So in the real manufactures, the advantage and disadvantage of Martensite should be considered comprehensively.

Acknowledgement

This work was based on cooperation between JWRI, Osaka University and Department of Mechanical Engineering, Tsinghua University. Authors would like to express the acknowledgement to Professor J. Pan, Professor A. Lu, Professor Y. Ueda and Professor K. Nakata for their kindly support.

References

1) David Tawfika, Peter John Muttonb, Wing Kong Chiua. Experimental and numerical investigations: Alleviating tensile residual stresses in flash-butt welds by localized rapid post-weld heat treatment. Journal of materials processing technology. Vol. 196, 2008, 279–291 [5]
2) H Mansouri, A Monshi, H Hadavinia. Effect of local induction heat treatment on the induced residual stresses in the web region of a welded rail. The Journal of Strain Analysis for Engineering Design. Vol. 39, No. 3, 2004, 271-283
3) David Tawfika, Oliver Kirsteinb, Peter John Muttonc, Wing Kong Chiua. Verification of residual stresses in flash-butt-weld rails using neutron diffraction. Physica B. Vol. 385–386, 2006, 894–896
4) Edward J. Kingston, Danut Stefanescu, Amir H. Mahmoudi, Chris E. Truman, David J. Smith. Novel Applications of the Deep-Hole Drilling Technique for Measuring Through-Thickness Residual Stress Distributions. Journal of ASTM International. Vol. 3, No.4, 2006, 146-157
5) A. Skyttebol, B.L. Josefson, J.W. Ringsberg. Fatigue crack growth in a welded rail under the influence of residual stresses. Engineering Fracture Mechanics. Vol.72, 2005, 271–285
6) H. Mansouri. A. Monshi. Microstructure and residual stress variations in weld zone of flash-butt welded railroads. Science and Technology of Welding and Joining. Vol. 9, No. 3, 2004, 237－245
7) Skyttebol Anders. Continuous Welded Railway Rails: Residual Stress Analyses, Fatigue Assessments and Experiments. Chalmers University of Technology. School of Mechanical Engineering. Department of Applied Mechanics. Sweden, 2004, Doctoral thesis
8) ZHANG Y H, ZHOU Q Y, CHEN Z Y, ZHOU Z G. Comparison of and Study on the External Quality of the Imported and Domestic Rails. China Academy of Railway Sciences. Vol.25, No.2, 2004, 97-100. (in Chinese)
9) LIU Fengshou, ZHANG Yinhua, CHEN Zhaoyang, ZHOU Qingyue. Characteristics of Continuous Cooling of UIC900A and U75V Rail Steel for Welding. China Academy of Railway Sciences.Vol.26, No.11, 2005, 63-68. (in Chinese)
10) Y Ueda, H Murakawa, Ninshu Ma. Numerical methods and codes for welding distortion and residual stress. Chengdu: Sichuan University Press, 2008, 11 (in Chinese)